

Investigating Asymptotic Suction Boundary Layers using a One-Dimensional Stochastic Turbulence Modeling Approach

Moritz M. Fragner

Department of Mechanical Engineering, Electrical
and Energy Systems
Brandenburg Technical University
Cottbus-Senftenberg
Siemens-Halske-Ring 14, Cottbus 03046, Germany
moritz.fragner@b-tu.de

Heiko Schmidt

Department of Mechanical Engineering, Electrical
and Energy Systems
Brandenburg Technical University
Cottbus-Senftenberg
Siemens-Halske-Ring 14, Cottbus 03046, Germany
schmidth@b-tu.de

ABSTRACT

The one-dimensional turbulence (ODT) model is applied to study asymptotic suction boundary layers. ODT offers fully resolved, unsteady simulations in one dimension. Turbulent three dimensional advection is represented through stochastic mapping events whose sequence is following a Poisson process. Because ODT is operating only in one dimension it features major cost savings compared to full 3D DNS and offers the potential to study asymptotic suction boundary layers at larger Reynolds numbers than currently feasible via DNS. In the current contribution we quantify the ability of the ODT method to simulate asymptotic suction boundary layers by comparing ODT results to recent DNS/LES findings. We focus on Reynolds numbers in the range $Re = u_\infty/v_0 \in [333, 400, 500]$, where u_∞ and v_0 are the freestream and suction velocity, respectively. We show that several features associated with suction boundary layers (reduced Reynolds stresses, high anisotropy near the wall, large friction Reynolds numbers) can be reproduced with ODT. In addition we investigate the influence of an important ODT model parameter, that influences the turbulent kinetic energy exchange between velocity components and hence impacts the predicted turbulent stress and isotropy profiles. Presented turbulent kinetic energy budgets will be discussed. We also conduct a resolution sensitivity study to demonstrate mesh convergence of our reference results.

INTRODUCTION

The mechanism of adding or removing mass through a porous surface (blowing or suction) has gained a lot of attention over the last decades, because it can provide a means to manipulate boundary layers in a favorable way. While wall blowing typically leads to a reduction in the exerted skin friction force, wall suction may stabilize boundary layers and thereby delay the onset of laminar-to-turbulent transition or separation of boundary layers. Another interesting feature of suction boundary layers is the existence of an asymptotic state, in which the boundary layer thickness becomes constant in the streamwise direction. Suction boundary layers were extensively studied via wind and water tunnel experiments by Antonia *et al.* (1988). Their results indicate, that turbulent stresses are significantly suppressed as a result of suction. The suppression affects the vertical and spanwise directions predominantly, hence leading to increased levels of anisotropy near the suction wall. These results could be confirmed by the first DNS simulations on suction boundary layers by Mariani *et al.* (1993). Subsequent DNS focusing on the initial relaxation of the flow after suction is introduced has been conducted by Chung & Sung (2001) and Chung *et al.* (2002), where rather long relaxation times are reported. In a recent DNS study (Kametani & Fukagata, 2011) it was argued that the suppression of turbulent stresses is a result of the mean convection overwhelming the turbulent contribution.

The asymptotic state, however, has rarely been observed in experimental investigations, because of the extraordinary tunnel sizes required. Large domain size and simulation time requirements have also limited the Reynolds number range to be studied via DNS or even LES simulations due to the extreme computational overhead implied. In a recent LES study (Bobke *et al.*, 2015) Reynolds numbers up to $Re = 500$ were considered, however box size independence of the results was only obtained up to $Re = 400$. The authors conclude, that the box size should exceed at least two boundary layers thicknesses in order to obtain box size independent results. In addition their results imply a large scale separation between the largest and smallest scales expressed by the large friction Reynolds number ($Re_\tau = \delta_{99}^+$) obtained in the suction case. This highlights the difficulty in resolving all the necessary scales in a three dimensional simulation. Thus a fully resolving DNS was only feasible for the lowest considered Reynolds number $Re = 333$ in their study.

In the current investigation, we use a different simulation approach, which is referred to as the one-dimensional turbulence model, ODT (Kerstein, 1999; Kerstein *et al.*, 2001; Ashurst & Kerstein, 2005). As the name implies, ODT operates only in one dimension, hence it offers substantial cost savings compared to three dimensional DNS/LES simulations and may provide the potential to study asymptotic suction boundary layers at larger Reynolds numbers. Like in DNS all required scales are resolved in ODT, however turbulent vortical overturns can not be simulated on a one-dimensional line. Instead these are represented through instantaneous mapping events, whose time sequence is described by a Poisson process. Location, size, and time of eddy occurrences are chosen according to a random process reflecting turbulent kinetic energy production mechanisms in the flow. In contrast to eddy viscosity models typically utilized in the RANS/LES framework, ODT can describe counter gradient turbulent diffusion and highly non-isotropic flows as present in the asymptotic suction boundary layer.

In the following we will compare ODT simulation results to the recent LES data by Bobke *et al.* (2015) for Reynolds numbers $Re \in [333, 400, 500]$. Additionally, a model parameter of ODT is extensively studied in here, that has a significant influence on the predicted anisotropy. A mesh sensitivity study will also be presented.

ODT MODEL BACKGROUND Governing Equation

The original formulation of ODT by Kerstein (1999) was later extended to include pressure scrambling effects (Kerstein *et al.*, 2001). ODT may be used for flows which display statistical homogeneity in two dimensions. In the remaining direction ODT can resolve gradients of the statistical and instantaneous quantities. Here we choose the ODT direction to be the wall normal direction (see Fig. 1), since in the asymptotic suction boundary layer flow statis-

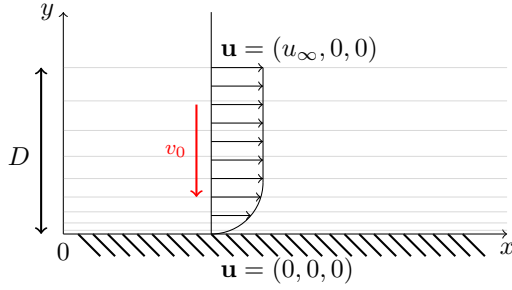


Figure 1. Graphic of the simulation set-up. The domain spans from the wall $y = 0$ out to the freestream $y = D$. A uniform suction towards the wall with velocity v_0 is applied.

tics are expected to vary only in this direction. The time evolution of the instantaneous 3D velocity vector field $\mathbf{u}(y, t)$ can then be formally described by the equation

$$\partial_t \mathbf{u}(y, t) + EE[\mathbf{u}(y, t), Y_0, L] = \nu \partial_y^2 \mathbf{u}(y, t) + v_0 \frac{\partial \mathbf{u}}{\partial y}. \quad (1)$$

The first term on the right-hand side represents the viscous diffusion of the flow involving the kinematic viscosity coefficient ν . In the suction boundary layer vertical mean advection towards the wall at constant advection velocity v_0 occurs, which is realized here via a source term, i.e. second term on the right hand side. Note that $v_0 \neq u_y$, since only the streamwise velocity component has a physical meaning in this model. The other velocity components of the velocity vector \mathbf{u} are introduced here only for energy redistribution purposes, see below. Turbulent advection is represented here by the operator EE which will be described next.

Eddy Implementation

The Operator EE on the left-hand side of Eq. 1 represents advection and pressure effects resulting from three dimensional turbulent eddies, that can not be simulated on the one-dimensional line. Instead this term is realized through instantaneous mappings, so called eddy events, which operate on the one-dimensional velocity profile.

Implementation of eddy events involves three ingredients: A permutation of fluid elements, a modification of the velocity profiles to allow for inter-component energy exchange and a selection mechanism of eddies that is dependent on the local flow state.

The permutation conserves the overall integral measures, such as momentum and energy, on a component basis. In addition the permutation is performed in a way that does not introduce discontinuities into the profiles. The simplest permutation map fulfilling these requirements is the triplet map (Kerstein, 1991). For a specified eddy with size L at location Y_0 this map compresses the original eddy section to one third, pastes three equal copies into the eddy range and reverses the middle copy. Outside of the eddy section, profiles remain unaffected. Mathematically the triplet map may be written as:

$$\hat{\mathbf{u}}(y, t) = \mathbf{u}(f(y), t) \quad (2)$$

where the mapping function $f(y)$ is

$$f(y) = Y_0 + \begin{cases} 3(y - Y_0) & \text{if } Y_0 \leq y \leq Y_0 + \frac{1}{3}L \\ 2L - 3(y - Y_0) & \text{if } Y_0 + \frac{1}{3}L \leq y \leq Y_0 + \frac{2}{3}L \\ 3(y - Y_0) - 2L & \text{if } Y_0 + \frac{2}{3}L \leq y \leq Y_0 + L \\ (y - Y_0) & \text{otherwise.} \end{cases} \quad (3)$$

Note that the triplet map conserves momentum and energy for each component separately. In reality, however, there is a continuous exchange of turbulent kinetic energy between velocity components, which is mainly driven by the turbulent pressure fluctuations in the flow. To capture such an exchange a second mechanism is introduced, which is referred to as the Kernel operation and may be written as an additional term added to the velocity profile as follows:

$$\hat{\mathbf{u}}(y, t) = \mathbf{u}(f(y), t) + \mathbf{c}K(y) \quad (4)$$

Here $K(y) = y - f(y)$ is the Kernel function, which is only non-zero within the eddy range and integrates to zero. Hence the Kernel does not change the overall components momentum, but it does change its energy. The integrated change in energy between pre and post eddy implementation for some component i is:

$$\Delta E_i = \frac{1}{2} \rho \int [u_i(f(y), t) + c_i K(y)]^2 - u_i^2(y, t) dy \quad (5)$$

where ρ in this study is a constant density of the flow. If the rhs expression of Eq. 5 is negative, energy is released from component i and maybe transferred to the other components j and k . The transfer is controlled by a model parameter α (transfer coefficient):

$$\Delta E_i = -\alpha Q_i + \frac{\alpha}{2} Q_j + \frac{\alpha}{2} Q_k \quad (6)$$

where the exchanged energy is expressed in terms of the maximum extractable energies Q_i . The latter corresponds to the minimum of Eq. 5 with respect to c_i :

$$Q_i = |\Delta E_i^{\min}| = \frac{1}{2\hat{K}} \rho L u_{i,K}^2 \quad (7)$$

where

$$u_{i,K} = \frac{1}{L^2} \int u_i(f(y), t) K(y) dy \quad (8)$$

and

$$\hat{K} = \frac{1}{L^3} \int K^2(y) dy \quad (9)$$

Equating Eq. 5 and Eq. 6 one can solve for the corresponding Kernel coefficient c_i . Note that by construction we have $\Delta E = \sum_i \Delta E_i = 0$, which implies that the Kernel does not change the overall energy of all components, just its distribution among them. The influence of the transfer coefficient α will be investigated in detail in this paper.

Eddy Selection

To implement an eddy as described in the last section a location Y_0 and eddy size L must be specified. These parameters are randomly sampled from a time-dependent joint distribution function $\lambda(Y_0, L, t)$ (eddy rate distribution), which specifies the number of eddies in the size range $[L, L + dL]$ and position range $[Y_0, Y_0 + dY_0]$ during a time interval dt . Technically eddies are implemented instantaneously. However, the mean time interval between implementations should be of the order of the physical eddy turnover time $\tau(L, Y_0, t)$ for the particular eddy:

$$\lambda(L, Y_0, t) = \frac{C}{L^2 \tau(L, Y_0, t)} \quad (10)$$

where the parameter C is another model parameter (rate coefficient), that controls the overall degree of turbulence. For a reasonable match to DNS/LES data we utilized $C = 10$ in this paper. The eddy turnover time $\tau(L, Y_0, t)$ is determined by the local flow state via eddy considerations:

$$\left(\frac{L}{\tau}\right)^2 \sim u_{1,K}^2 + u_{2,K}^2 + u_{3,K}^2 - Z \frac{v^2}{L^2} \quad (11)$$

where $u_{i,K}$ is given by Eq. 8 and therefore is related to the shear in the velocity field, because this integral increases as more shear is introduced in the velocity field. This implies that the probability of eddy implementation, i.e. turbulence, scales with the velocity gradients. This relationship between turbulence and velocity shear is analogue to the Ansatz commonly used for eddy viscosity models in the RANS/LES framework, which relates the mean effect of turbulence (i.e. Reynolds stresses) to the gradients of the filtered velocity field. Here, however, the relationship is applied for individual eddy events rather than for some mean quantity. Note that, because each eddy event increases the velocity gradients via the triplet map, the probability of another, smaller eddy at that location is correspondingly increased. This leads to implementation of successively smaller eddies and therefore can resemble the dynamics of an eddy energy cascade.

The last term on the rhs of Eq. 11 was originally introduced to suppress small eddies, that are smaller than the Kolmogorov length scale (i.e. $Z = 1$). In wall bounded flows, however, increasing the size threshold for eddy suppression is important for obtaining reasonable fits of velocity profiles to DNS data, due to unresolved 3D features in ODT (Meiselbach, 2015). Here we used $Z = 400$, which implies that eddies with associated turnover velocities smaller than 20 Kolmogorov velocity scales are suppressed.

Integrating the eddy rate distribution $\lambda(L, Y_0, t)$ over all possible L and Y_0 defines the mean event rate $R(t) = \int \int \lambda(L, Y_0, t) dL dY_0$. Then the eddy sampling process describes a Poisson process with mean rate $R(t)$ at time t . The mean rate and the eddy rate distribution are time dependent via the link to the local flow state, i.e. Eq. 11. This implies, that the eddy rate distribution needs to be frequently reconstructed, which becomes prohibitively expensive. To overcome this problem a much more efficient but mathematically equivalent procedure is applied, which is referred to as the over-sampling algorithm with combined thinning. For more details see Kerstein (1999); Schmidt *et al.* (2003).

SIMULATION SETUP

In the stationary and laminar case, the left hand side of Eq. 1 is zero. Integrating the remaining equation twice gives:

$$u(y) = u_\infty \left(1 - \exp\left(-\frac{yv_0}{v}\right)\right) \quad (12)$$

which is used here as initial condition for the streamwise component. The other components are initialized to zero. Furthermore, we apply Dirichlet boundary conditions as $(u_\infty, 0, 0)$ and $(0, 0, 0)$ in the freestream ($y = D$) and at the wall ($y = 0$), respectively (see Fig. 1). The Reynolds number based on the laminar displacement thickness $\delta_0 = v/v_0$ becomes:

$$Re = \frac{u_\infty \delta_0}{v} = \frac{u_\infty}{v_0} \quad (13)$$

When varying this Reynolds number, the suction velocity v_0 was kept constant. Because ODT simulates the instantaneous flow state in time, ensemble averaging needs to be applied to obtain converged statistics. Here we employ 96 realizations computed in parallel on 96 cores. Starting from the laminar profile (Eq. 12) the simulations are evolved for a transient phase until the flow has reached statistical stationarity as indicated by the converged boundary layer thickness δ_{99} . After the transient phase we apply an averaging phase of $2.5 \cdot 10^5$ time scales $t_C = \delta_0/u_\infty$. The right hand side terms of Eq. 1 are solved using an implicit solver to avoid restrictive time step constraints. In the following we studied the asymptotic suction boundary layer for various Reynolds numbers, but also investigated the effect of varying the transfer coefficient α and the mesh resolution. The details are given in Table 1.

Table 1. Table of the simulations performed. Indicated are the Reynolds number Re , Domain length D , min/max mesh cell sizes in viscous units, and the transfer coefficient α .

Run	Re	D	Δy_{min}^+	Δy_{max}^+	α
<i>Re333</i>	333	500	0.34	43	0.1
<i>Re400</i>	400	500	0.34	43	0.1
<i>Re500</i>	500	1000	0.34	43	0.1
<i>A1</i>	400	500	0.34	43	0.667
<i>A2</i>	400	500	0.34	43	1.0
<i>MIN1</i>	400	500	0.17	43	0.1
<i>MIN2</i>	400	500	0.68	43	0.1
<i>MIN3</i>	400	500	1.7	43	0.1
<i>MAX1</i>	400	500	0.34	21.5	0.1
<i>MAX2</i>	400	500	0.34	86	0.1
<i>MAX3</i>	400	500	0.34	215	0.1

VARIATION OF REYNOLDS NUMBER

In this section the results for variation of the Reynolds number $Re \in [333, 400, 500]$ will be discussed, i.e. runs *Re333*, *Re400* and *Re500* in Table 1.

After the transient phase, the final values for the boundary layer thickness and the corresponding turbulent friction Reynolds numbers $Re_\tau = \delta_{99}^+$ are calculated and tabulated in Table 2 where they can be directly compared to DNS/LES data from Bobke *et al.* (2015). It may be seen that the ODT predicted values match the DNS/LES counterparts very closely, with a relative difference of

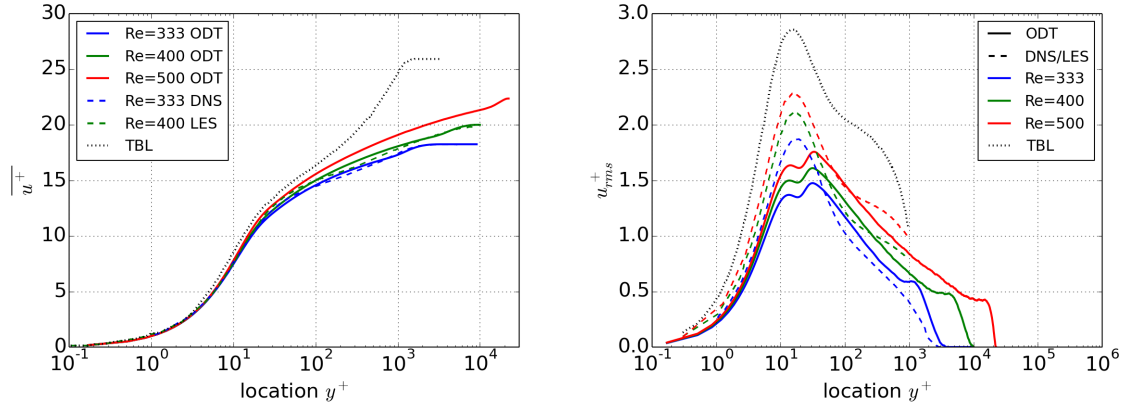


Figure 2. Left: Mean velocity profiles in viscous units. Right: Streamwise stresses in viscous units. The data for the spatially evolving boundary layer (TBL) is also displayed for $Re_\theta = 4300$ from Schlatter & Örlü (2010).

Table 2. Output table of the simulations performed. Displayed are the boundary layer thickness δ_{99} (in units of the laminar displacement thickness δ_0), turbulent friction Reynolds number $Re_\tau = \delta_{99}^+$ and Von Kármán constant κ . The DNS/LES reference from Bobke *et al.* (2015) is also given.

Run	δ_{99}	Re_τ	κ
<i>Re333</i>	104	1906	0.91
<i>Re400</i>	296	5924	0.77
<i>Re500</i>	813	18189	0.67
<i>A1</i>	193	3857	0.71
<i>A2</i>	76	1515	0.68
<i>MIN1</i>	286	5711	0.76
<i>MIN2</i>	273	5470	0.78
<i>MIN3</i>	240	4804	0.81
<i>MAX1</i>	291	5823	0.77
<i>MAX2</i>	276	5529	0.77
<i>MAX3</i>	275	5528	0.74
<i>DNS333</i>	92	1680	0.89
<i>LES400</i>	287	5230	0.82

$\sim 10\% - 13\%$ in the reported numbers. Note that the displayed turbulent friction Reynolds numbers are comparatively large compared to the spatially evolving boundary layer without suction, which implies a large scale separation between the large scales and the viscous transport scales. For example comparing Re_τ at equivalent momentum thickness Reynolds numbers to the spatially evolving case (Schlatter & Örlü, 2010), we find that the reported Re_τ in the suction case is larger by a factor of ~ 3 for the Reynolds numbers displayed.

After the transient phase, a time-averaging phase for all 96 realizations is applied to obtain converged velocity statistics. The mean and rms profiles scaled in viscous units are displayed in Fig.2 along with plots for the corresponding DNS/LES data and the spatially evolving

boundary layer without suction (TBL).

While the inner layer is found to scale independent of Reynolds number, the freestream velocities scale as \sqrt{Re} when displayed in viscous units. It may also be seen, that the freestream is reached at considerably larger y^+ values compared to the spatially evolving boundary layer without suction. This implies a smaller slope in the log region, or correspondingly larger values for Von Kármán constants κ , which are also tabulated in Table 2. The agreement with the DNS/LES data is reasonably good. As the suction velocity is reduced (larger Reynolds numbers), the Von Kármán constant is reduced and approaches the standard value.

Compared to the DNS/LES reference streamwise stresses are consistently under predicted by ODT, a feature that has been observed in previous applications of ODT to the channel flow problem (Meiselbach, 2015). Interestingly, while the correct amount of mixing is provided, as indicated by the close agreement of the Von Kármán constants, the turbulent stresses are yet under predicted by ODT. One should keep in mind, however, that ODT can not represent the elongated turbulent structures actually occurring near the suction wall, since this would require three dimensional flow information to be incorporated into the model. As suggested by Schmidt *et al.* (2003), a coupling of an array of ODT lines with a coarse grained LES simulations (commonly referred to as ODTLES) may remove the observed artifact. Additionally, there is a small dip seen in the peak of the stress profiles, which is another artifact caused by the triplet map morphology (Lignell *et al.*, 2013). It can also be seen that the stress amplitudes decrease as the Reynolds number is reduced (or equivalently the suction velocity is increased). This implies that suction suppresses turbulent stresses and therefore confirms a well known result from earlier experiments (Antonia *et al.*, 1988). Hence the peak stress amplitudes stay always below the corresponding peak of the spatially evolving boundary layer without suction.

TRANSFER COEFFICIENT α

In this section we analyze the effect of the transfer coefficient α . Hence we compare runs *Re400*, *A1* and *A2* from Table 1 in this Section. Earlier in this paper it was shown that this parameter controls the transfer of turbulent kinetic energy between the velocity components. Here $\alpha = 0$ would neglect such an energy exchange, $\alpha = 1$ would result in the maximum exchange possible, and $\alpha = 2/3$ causes equipartition of energies and hence models the tendency of the flow towards isotropy.

As Table 2 indicates, increasing the value of α increases the slope of the velocity in the log region (reduced κ) with the consequence that

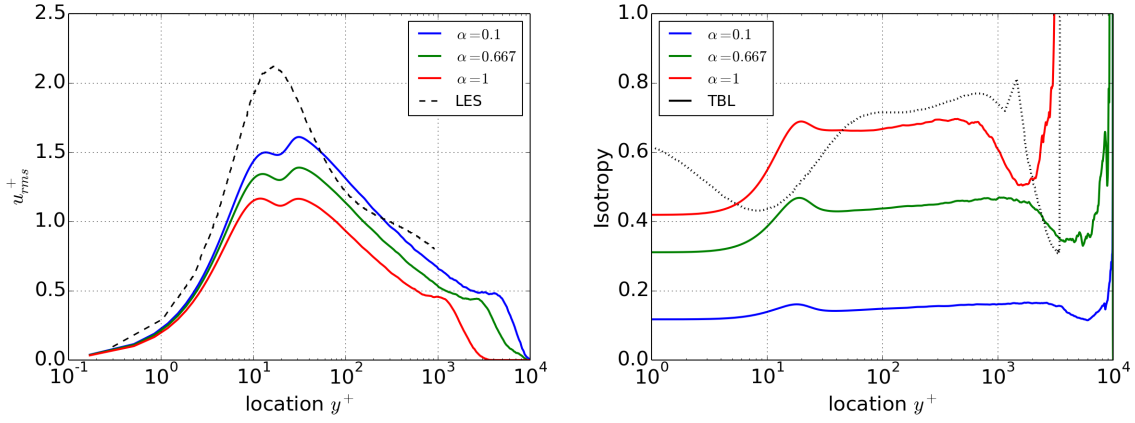


Figure 3. Left: Streamwise stresses for the three parameter values varied. The LES reference is also indicated. Right: Isotropy profiles, where this is calculated as the ratio of spanwise to streamwise stress component. The profile for the spatially evolving boundary layer (Schlatter & Örlü, 2010) is also indicated (TBL).

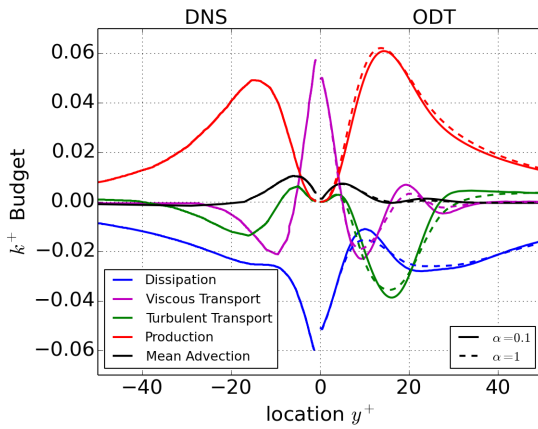


Figure 4. Budgets driving the evolution of turbulent kinetic energy. Displayed for two values of α . The DNS reference is for $Re = 333$. On the right hand side, results for runs $Re400$ and $A2$ are displayed.

the freestream is attained at smaller y^+ values which in turn leads to reduced values of the boundary layer thickness δ_{99} and friction Reynolds numbers Re_τ . Fig. 3(left) shows the streamwise stress profiles for the three parameter values applied. Since the source of turbulent kinetic energy is provided mainly by shear in the streamwise velocity component, almost all of the turbulent stresses would accumulate in the streamwise component, if no transfer would be allowed ($\alpha = 0$). As the parameter α is increased a larger fraction of this turbulent kinetic energy gets transferred to the other components, thereby reducing the peak stresses of the streamwise component as is visible from Fig. 3(left).

Correspondingly the isotropy, which is defined as the ratio of the spanwise to streamwise stress, is increased for increased values of α . This maybe seen from Fig. 3(right), where we also show the profile for the spatially evolving boundary layer without suction. It may be seen that for all values of α reduced levels of isotropy are reported near the wall when suction is introduced. This is a well known feature of suction boundary layers (Antonia *et al.*, 1988; Mariani *et al.*, 1993; Bobke *et al.*, 2015). Note that at lower Reynolds number ($Re = 333$) the best agreement with corresponding DNS was obtained for $\alpha = 2/3$ (not shown) in the inner layer, while in the outer layer ($y^+ > 100$) the α parameter should be in-

creased to obtain better agreement.

In Fig. 4 we also compare the budget terms for the turbulent kinetic energy for runs $Re400$ and $A2$ against the DNS reference results (which here are provided for $Re = 333$ from Bobke *et al.* (2015)). The overall agreement of the budget terms is reasonable, given that the Reynolds numbers are slightly different. Turbulent production, viscous transport, and mean advection show only slight discrepancies compared to the DNS reference. A much larger difference may be seen in the dissipation profile, which shows reduced dissipation magnitudes in a region of high production, which instead is attributed to increased levels of turbulent transport. It is explained by the fact, that the viscous dissipation term is only resolved in the wall normal direction, while the streamwise and spanwise dissipation terms remain unresolved. Comparing the dissipation for the two values of α , we can observe that the situation improves slightly, when more energy is transferred to the other velocity components ($\alpha = 1$). It is possible that the energy in the spanwise and vertical velocity components is associated with an increased variance of velocity gradients, hence leading to more efficient dissipation.

MESH CONVERGENCE STUDY

In this last section we want to demonstrate mesh convergence of our results by presenting simulations at higher and lower resolutions. All simulations have been performed using an adaptive version of ODT (Lignell *et al.*, 2013) which features dynamic mesh adaption based on a conservative scheme, that refines regions of high gradients and curvature. The simulations so far discussed employ a maximum and minimum mesh cell size of $\Delta y_{\max}^+ = 43$ and $\Delta y_{\min}^+ = 0.34$, respectively (see Table 1). Here Δy_{\min}^+ is mainly applied in regions close to the wall. The run $Re400$ serves again as the reference run. In run $MIN1$ and $MAX1$ we increased the resolution, by reducing Δy_{\min} and Δy_{\max} by a factor of two, respectively. In run $MIN2$ and $MAX2$ we increased the corresponding mesh cell sizes by a factor of two, in runs $MIN3$ and $MAX3$ we increased them by a factor of five.

From Table 2, we can see, that the effect of changing the largest cell sizes (Δy_{\max}) shows only little influence on the attained boundary layer thickness. On the other hand, the boundary layer thickness displays a much larger sensitivity to a reduction of the finest resolution, which is applied near the wall (Δy_{\min}). A five-fold increase of Δy_{\min} leads to considerable smaller boundary layers. This is consistent with the stress profile displayed in Fig.5, which demonstrates that the peak turbulent stresses can become suppressed significantly, if a too low resolution is applied near the wall.

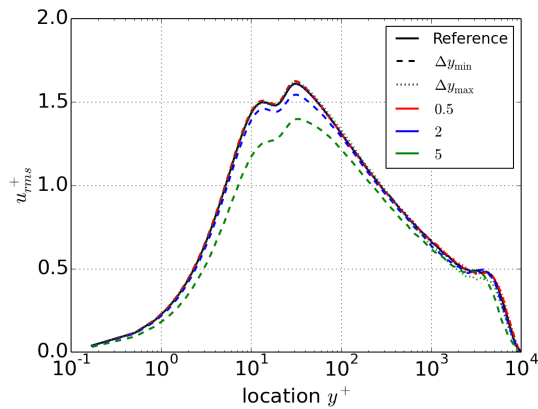


Figure 5. Streamwise stress profiles. Displayed for increased resolution (red) and lower resolution (blue, green) by multiplying Δy_{\min} (dashed) or Δy_{\max} (dotted) with the factor indicated.

It may also be verified, that reducing Δy_{\min} or Δy_{\max} by a factor of two does not show any difference to our reference simulation, i.e. the curves for the higher resolution are indistinguishable to the reference case. This indicates, that the resolution that we have chosen is already within the mesh converged region and therefore sufficient.

CONCLUSION

In this paper we have tested the ability of the ODT method to simulate asymptotic suction boundary layers. We have performed simulations for various Reynolds numbers in the range $Re \in [333, 400, 500]$ and compared our results to recent DNS/LES data. In addition we investigated the effect of varying an important ODT model parameter, α , which controls the transfer of turbulent kinetic energy between velocity components. A resolution sensitivity study was also conducted. The following key results were found:

- ODT matches the DNS/LES reference results reasonable well in terms of the attained boundary layer thickness, turbulent friction Reynolds number, and Von Kármán constants.
- Turbulent stresses are consistently underpredicted by ODT.
- Several features of asymptotic suction boundary layers were reproduced, i.e. reduced Reynolds stresses, high anisotropy near the wall and large friction Reynolds numbers.
- Turbulent kinetic energy budgets compare well to DNS data, except for the dissipation profile, which is well known and might be explained by the fact that ODT misses the off-line dissipation terms.
- The transfer coefficient α influences a back to isotropy tendency of the model on small scales. The discrepancy of the dissipation profile can be slightly improved for increased values of α .
- Lowering the near wall resolution has significant degrading effects on turbulent stresses and attained boundary layer thickness. Increasing the resolution showed nearly no influence, indicating that mesh convergence was reached in our simulations.

To conclude, ODT is a model that is quite capable to simulate asymptotic suction boundary layers and provides detailed flow information. Despite some discrepancies to the DNS/LES seen, one has to keep in mind that ODT operates in one dimension only, and therefore offers huge cost saving compared to equivalent DNS/LES. For example, the ODT domain contains up to ~ 500 cells at $Re = 400$, while comparable LES simulations by Bobke *et al.* (2015) for that Reynolds number contain up to 10^8 cells.

REFERENCES

- Antonia, R.A., Fulachier, L., Krishnamoorthy, L.V., Benabid, T. & Anselmet, F. 1988 Influence of wall suction on the organized motion in a turbulent boundary layer. *Journal of Fluid Mechanics* **190**, 217–240.
- Ashurst, Wm. T. & Kerstein, A.R. 2005 One-dimensional turbulence: Variable-density formulation and application to mixing layers. *Physics of Fluids* **17**.
- Bobke, A., Örlü, R. & Schlatter, P. 2015 Simulations of turbulent asymptotic suction boundary layers. *Journal of Turbulence* **17**, 157–180.
- Chung, Y.M. & Sung, H.J. 2001 Initial relaxation of spatially evolving turbulent channel flow with blowing and suction. *AIAA Journal* **39**, 2091–2099.
- Chung, Y.M., Sung, H.J. & Krogstad, P. 2002 Modulation of near-wall turbulence structure with wall blowing and suction. *AIAA Journal* **40**, 1529–1535.
- Kametani, Y. & Fukagata, K. 2011 Direct numerical simulation of spatially developing turbulent boundary layers with uniform blowing or suction. *Journal of Fluid Mechanics* **681**, 154–172.
- Kerstein, A.R. 1991 Linear-eddy modeling of turbulent transport. part 6. microstructure of diffusive scalar mixing fields. *Journal of Fluid Mechanics* **231**, 361–394.
- Kerstein, A.R. 1999 One-dimensional turbulence: model formulation and application to homogeneous turbulence, shear flows, and buoyant stratified flows. *Journal of Fluid Mechanics* **392**, 277–334.
- Kerstein, A.R., Ashurst, W.T., Wunsch, S. & Nilsen, V. 2001 One-dimensional turbulence: vector formulation and application to free shear flows. *Journal of Fluid Mechanics* **447**, 85–109.
- Lignell, D.O., Kerstein, A.R., Sun, G. & Monson, E.I. 2013 Mesh adaption for efficient multiscale implementation of one-dimensional turbulence. *Theoretical and Computational Fluid Dynamics* **27**, 273–295.
- Mariani, P., Spalart, P. & Kollmann, W. 1993 Direct simulation of a turbulent boundary layer with suction. *So RMC, Speciale CG, Launder BE, editors. Near-wall turbulent flows* pp. 347–356.
- Meiselbach, F. 2015 Application of ODT to turbulent flow problems. PhD thesis, BTU Cottbus-Senftenberg.
- Schlatter, P. & Örlü, R. 2010 Assessment of direct numerical simulation data of turbulent boundary layers. *Journal of Fluid Mechanics* **659**, 116–126.
- Schmidt, R.C., A.R., Kerstein, Wunsch, S. & Nilsen, V. 2003 Near-wall les closure based on one-dimensional turbulence modeling. *Journal of Computational Physics* **186**, 317–355.